PRZEGLĄD SPAWALNICTWA
Welding
TECHNOLOGY REVIEW

Original Article

Sliding of spherical ball on solid lubricating coating combined with wear process

Marcin Białas [1,*] iD **, Jan Maciejewski** [2] iD **, Stanisław Kucharski** [3] iD

[1] Faculty of Production Engineering, Warsaw University of Technology, Poland
[2] Faculty of Automotive and Construction Machinery, Warsaw University of Technology, Poland
jan.maciejewski@pw.edu.pl
[3] Institute of Fundamental Technological Research, Polish Academy of Sciences, Poland
skuchar@ippt.pan.pl
* Correspondence: dr hab. inż. Marcin Białas; marcin.bialas@pw.edu.pl

Abstract: In present paper we show results of ball-on-disk wear experiment of MoS_2 film deposited on Ti6Al4V substrate. The ball material is aluminium oxide. The tests are performed for different surrounding temperature conditions: 20°C, 200°C and 350°C. It is shown that depth of the wear groove increases with increasing surrounding temperature. A finite element modelling approach is next developed to mimic the experimental observations of ball-on-disk wear process. It is based on the assumption of steady state condition developed during short time scale at contact region. The steady state results can next be applied to long time scale in which wear process is numerically simulated. Model results are compared with experimentally obtained wear groove and show satisfactory agreement.

Introduction

Wear at contact interfaces is connected with several thermo-mechanical phenomena such as: variation of friction coefficient with contact stress and temperature, variation of mechanical properties with temperature, local temperature distribution affected by frictional sliding. Many of these aspects were analysed by a number of researchers, see for example [1,2,3]. In these papers configurational changes were considered for different boundary conditions, including ball on disc tests. Using finite elements or other numerical methods evolution in stress state and temperature field due to wear was modelled. The contact shape evolution during wear process of two bodies in relative sliding motion was usually simulated numerically by integrating wear rate expressed in terms of the relative sliding velocity and the contact pressure. A steady state was then predicted in the case of constant contact zone by the incremental integration procedure accounting for contact shape and pressure variation. A more effective procedure was developed in [4,5] by postulating minimization of the contact response functional. It was demonstrated that the stationary conditions of the total wear dissipation power at the contact interface provide the pressure distribution in the steady wear. They generate the co-axiality rule requiring the wear rate vector to be collinear with the wear velocity vector consistent with the boundary conditions allowing for a rigid body motion induced by the wear process. The experimental and numerical results of wear for the reciprocal ball sliding on a plate substrate is presented in the paper [6]. The numerical time integration of the wear rule was performed in order to specify wear parameters for modified Archard's rule. In the identification procedure, the wear coefficient appeared to depend on the sliding length. By minimization of the squared distance between experimental and modelling curves it was possible to find the wear parameters. Contact of rough surface with different topographies against a rigid plane was analysed in the paper [7]. Statistical approach and FEM for modelling of contact were applied. 3D surface topographies were measured in initial and deformed state using scanning profilometry. An experimental procedure was designed that enabled specifying load-approach and load-real contact area relations corresponding to plastic deformation of roughness zone. In the paper [8] analysis of coupled friction and wear process in sliding along the rough surface with an anisotropic asperity pattern characterized by single or mutually orthogonal striations is presented. Due to wear process the initial anisotropic response evolves with the variation of asperity distribution, tending to a steady-state pattern.

In [9] typical conditions are reviewed in which low friction coatings are sought as well as the demands for properties which coatings should fulfil in order to function in an appropriate way. An example of such coatings for use in a vacuum is based on molybdenum disulphide (MoS_2). Self-lubricating coatings with MoS_2 exhibit low friction and are used in the great majority of applications requiring solid lubrication. As examples we could mention cutting tools such as drills and saws, highly loaded gear wheels made of titanium alloys, sliding and roller bearings, cast iron pistons in radial piston motors, piston rings and home appliances including refrigerant compressors, washers and dryers.

The structure of MoS_2 is layered. Atoms belonging to one layer are strongly bonded by covalent interactions. There are van der Waals bonds between the layers which are weak and result in sliding at adjacent sulphur planes. Quasiamorphous MoS_2Ti composite coatings, where Ti is added to molybdenum disulphide, are more adhesive, denser and more oxidation resistant than pure MoS_2. The effect of deposition parameters and Ti content on crystallographic orientation and friction coefficient and wear rate in MoS_2Ti was examined in [10]. The wear resistance and friction coefficient of the MoS_2Ti coated Ti-6Al-4V alloy was investigated at various temperatures in the paper [11]. It was shown that the presence of the MoS_2Ti coating decreases the friction coefficient from 0.85 to 0.15. The coating essentially increases the wear resistance of the alloy at room temperature. Review paper [12] compiles publications from last seventy years about the research developments in metal matrix self-lubricating composites containing MoS_2. Information on the tribological properties of such composites according to the varied matrixes, contents, processing conditions, testing temperatures and atmospheres are discussed.

In the paper we show experimental results of a ball on disk test, where MoS_2 film deposited on Ti6Al4V is subjected to wear process by contact with a sapphire ball. Several surrounding temperatures and ball loading forces are used. Results of finite element modelling of wear process are shown next. Assuming thermo-elastic material we perform coupled thermo-mechanical analysis resulting in steady state at the contact interface. Obtained stress profile is next applied to simulate wear and with a new wear profile new steady state is sought. Procedure is repeated until desired simulation time is reached. Experimental findings are compared with finite element results.

Ball-on-disk-tests

Unlubricated ball-on-disk tests were performed as specified in Figure 1 using home-made wear tester. The ball was made of aluminum oxide Al_2O_3 and had a diameter of 6 mm. The disk was made of Ti6Al4V titanium alloy deposited with MoS_2 coating of thickness 3 μm. Depending on experiment specification the ball was loaded either by force equal 1 N or 5 N. Three different surrounding temperature conditions were considered, namely 20 °C, 200 °C and 350 °C. The slip was achieved by sample (disk) rotation with respect to the counter-sample (ball). The number of cycles was 20000 with one disk rotation per second. Rotation diameters are summarized in Table I together with other experiment details.

Both the topographies of unworn outer surface of MoS_2 layer and of subsequent wear tracks were measured using a scanning profilometer Hommel Tester T8000 Nanoscan. All roughness parameters were determined using Hommel Map software for surface analysis. Table II presents roughness parameters obtained for unworn surface and taken from square area measurement of side dimension equal to 0.5 mm. Figure 2 presents exemplary roughness profile of examined sample. It should be noted that peak heights can reach values of around 0.8 μm but the arithmetic mean height Sa and root mean square height Sq are only 0.0853 μm and 0.138 μm, respectively. This shows that some asperities can be significantly bigger than others but the number of them is limited, since their dimensions do not influence values of Sa and Sq.
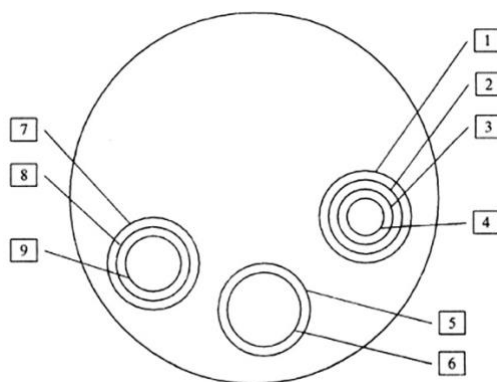
Fig. 1. Specification of ball on disc tests

Table I. Specification of ball-on-disk experiments. Tests with no data were trial experiments

Test number	Loading force [N]	Rotational diameter [mm]	Test temperature [°C]
1	1	7.2	RT
2	1	6.2	RT
3	1	5.8	RT
4	–	–	–
5	1	7.5	200
6	5	5.2	200
7	5	9.2	350
8	1	7.5	350
9	–	–	–

Table II. 3D surface parameters of unworn MoS$_2$ layer

Parameter (ISO 25178)	Value [µm]	Description
Sq	0.138	Root mean square height
Ssk	1.51 [–]	skewness
Sku	75.6 [–]	kurtosis
Sp	1.08	Maximum peak height
Sv	9.09	Maximum pit height
Sz	10.2	Maximum height (range)
Sa	0.0853	Arithmetic mean height
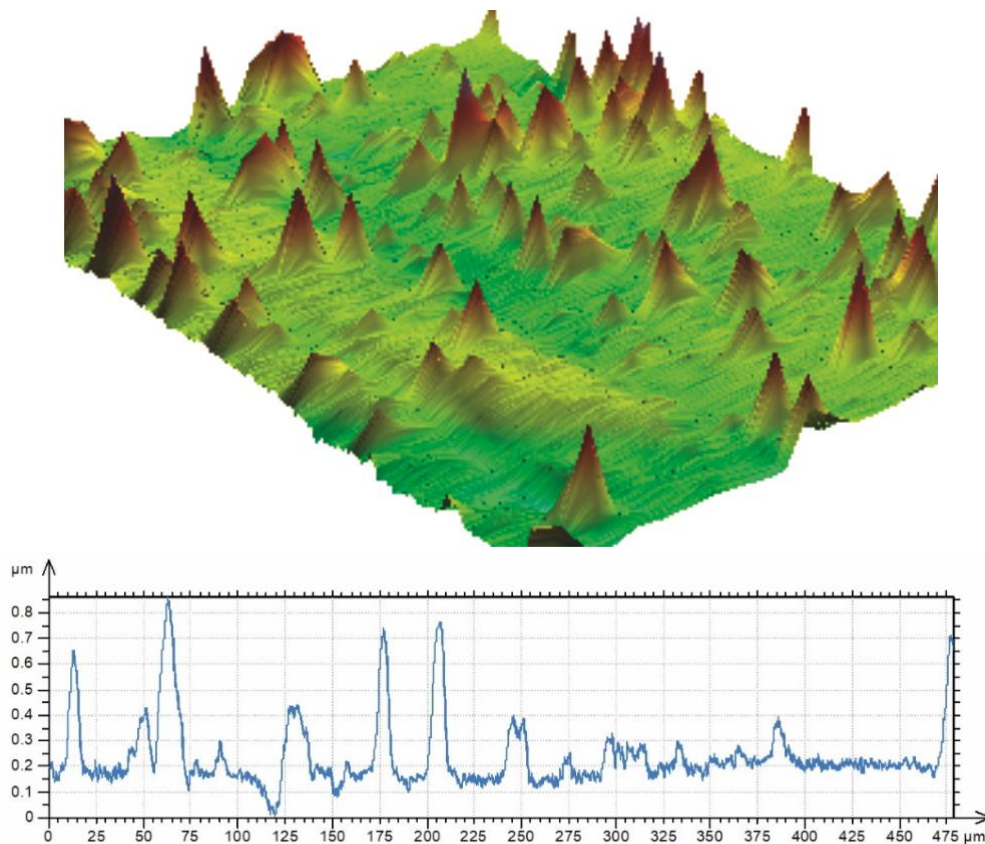
Fig. 2. Exemplary unworn profile of MoS$_2$ surface

Figure 3 presents roughness profile of the sample after room temperature ball-on-disk experiments, Tests from 1 to 3. Three different wear groves are indicated. Applied loading force was 1 N for all cases. It can be seen that the wear grooves are small when compared to surface asperities. The maximum observed

depth is about 200 nm. The groove resulting from Test number 2 is difficult to be distinguished among neighboring asperities. Figure 4 shows zoom-ins of wear profiles resulting from Tests number 1 and 3. One can see that the grooves are very uneven. Small flashes existing around them are also visible. Table III summaries average mean and maximum values of groove depths calculated from seven different cross-sections for each test. The average depth varies from 0.15 μm to 0.20 μm.
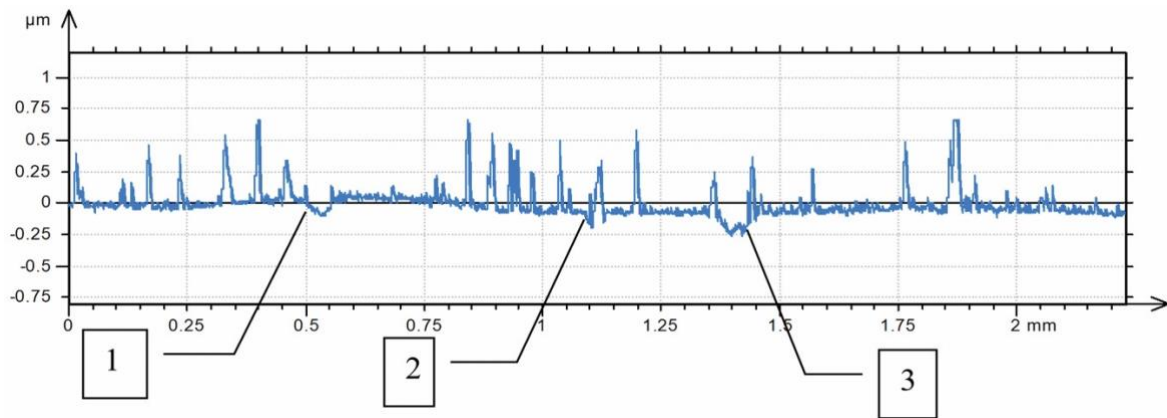
Fig. 3. Roughness profile after ball-on-disk test at room temperature. Indicated grooves from Tests 1, 2 and 3

(a)   (b)
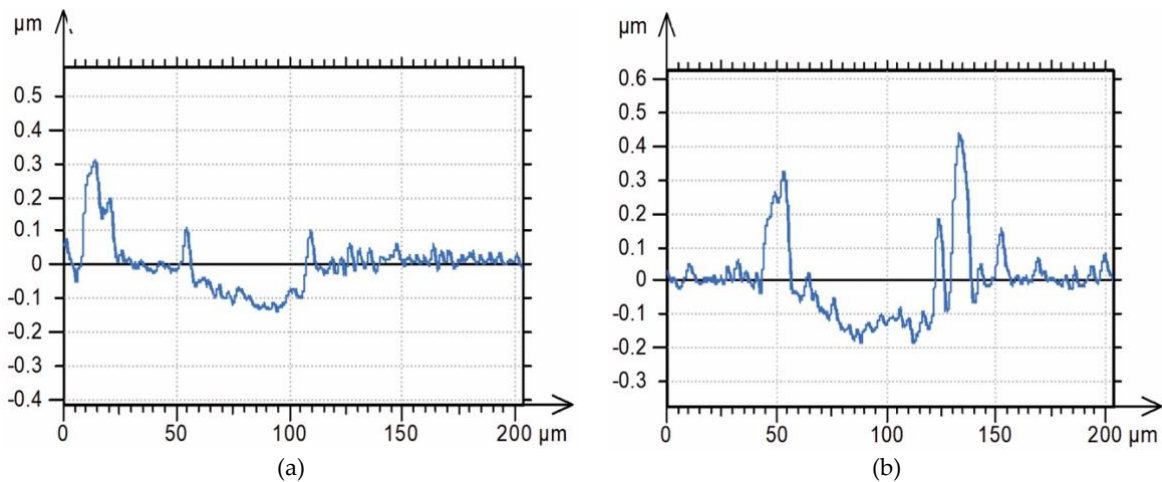
Fig. 4. a) Wear groove from Test 1. b) Wear groove from Test 3

The second set of ball-on-disk experiments was performed at surrounding temperature of 200 °C, Tests number 5 and 6 in Table I with loading forces equal respectively 1N and 5N. Figure 5(a) presents topography of outer surface with indicated wear tracks and Figure 5(b) shows roughness profile along a cross-section. Similarly to the previous set of tests, Table IV summaries average, mean and maximum values of groove depths based on analysis of eleven locations for each wear track. Average depth of wear track for loading force of 1N is 0.29 μm, which is not much higher than observed for the same loading during room temperature experiments. The height of the flashes is about 0.4 μm.

Table IV. Groove depths for Tests 5 and 6 temperature 200 ℃

	Test 5	Test 6
Average [μm]	0.29	0.43
Minimum [μm]	0.17	0.3
Maximum [μm]	0.4	0.56

Depth and shape of wear track are significantly different for Test number 6 obtained by 5N ball loading. The average depth now is about 0.43 μm, neighboring flashes have heights similar in value to the track depth. It can be stated that depth is rather uniform. Occasionally isolated island can be seen, which divide the groove bottom in half, see Figure 6(a). As can be seen in Figure 6(b) the groove bottom away from the islands is mostly flat with parameter Ra equal to 17 nm and Rq equal to 20.3 nm, the distance from maximum peak top to minimum valley bottom does not exceed 100 nm. The flat part of wear groove has width of about 70 μm.
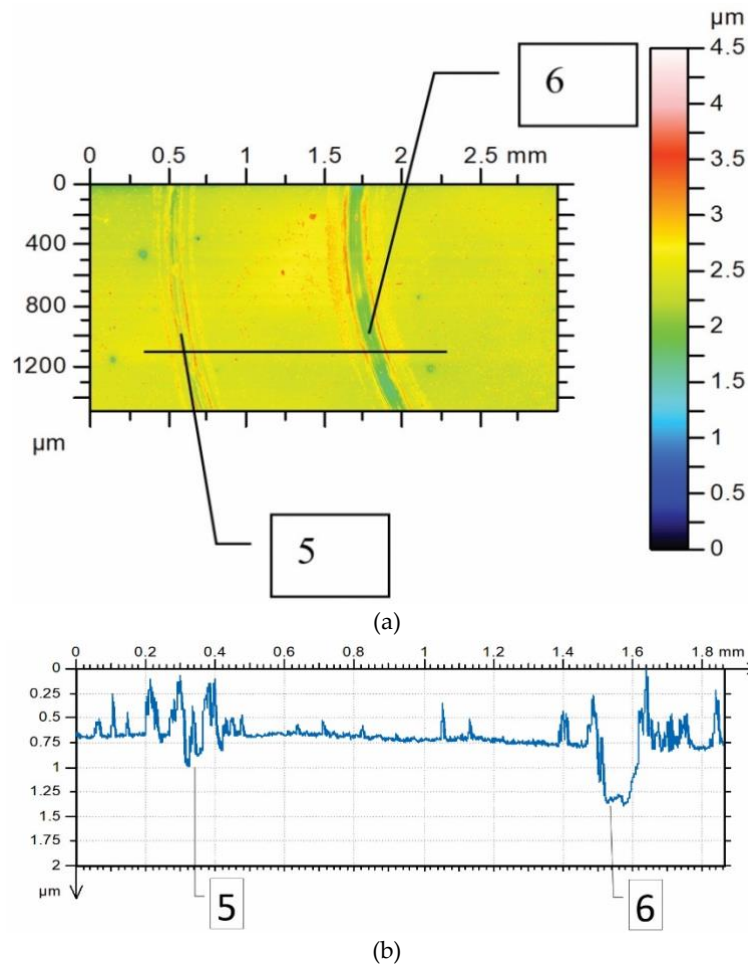
Fig. 5. a) Roughness topography after ball-on-disk test at temperature 200 °C with indicated grooves from Tests 5 and 6. Straight line indicates location of profile cross-section. b) Roughness topography along indicated cross-section
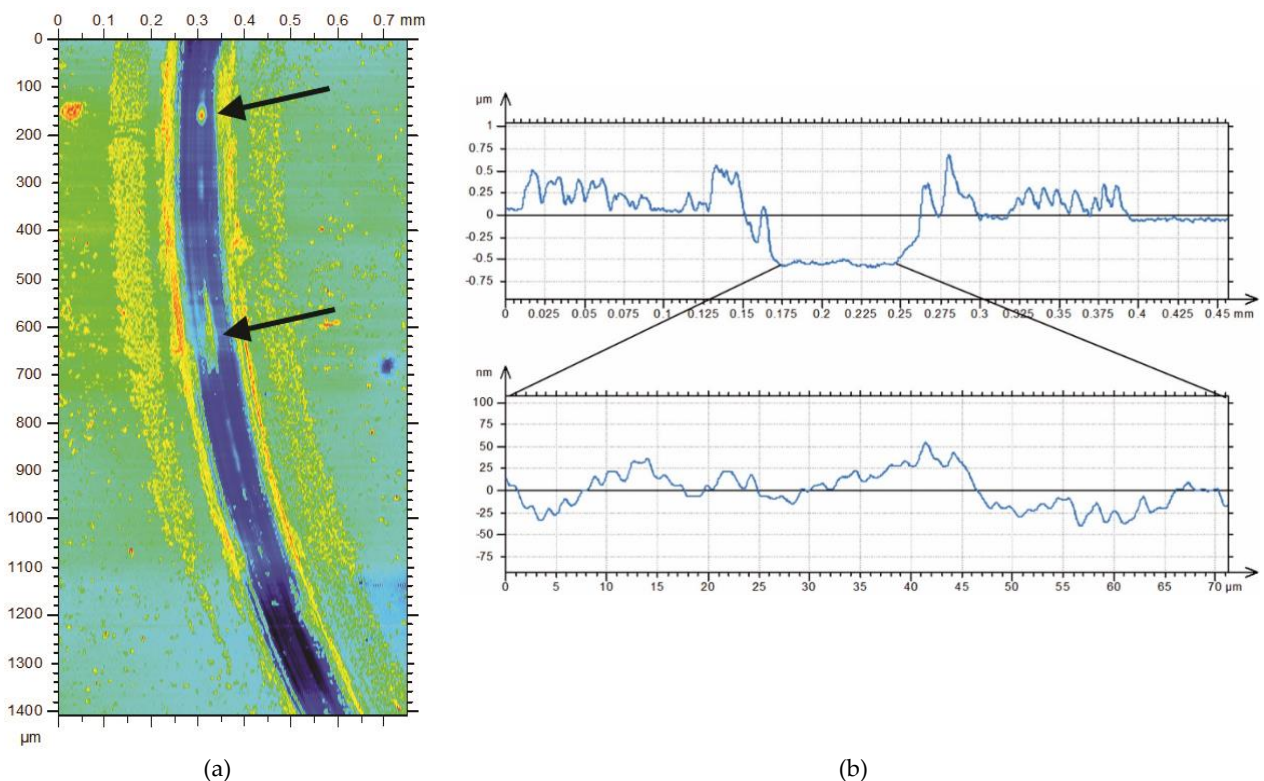
Fig. 6. Test 6 carried out in temperature 200 °C. a) Roughness topography with arrows indicating islands in groove bottom. b) Cross section through groove bottom away from the islands

The third set of ball-on-disk experiments was performed at surrounding temperature of 350 °C, Tests number 7 and 8 in Table I with loading forces equal respectively 5 N and 1 N. Figure 7 presents topography of outer surface with indicated wear tracks along three different cross-sections. In general, for both Tests 7 and 8 there are hardly any flashes visible. One can observe the increase of groove depths in comparison to the results obtained for corresponding forces during experiments performed at surrounding temperature of 200 °C. The maximum depth for loading force of 5N is now 2.8 μm, for 1N it is about 2.2 μm. Table V summaries average mean and maximum values of groove depths based on analysis of seven cross-sections for each wear track. For loading force of 1N the average depth of wear tracks is close to the maximum value. Figure 8 presents zoom-in of groove bottom for Test 7 (5N) at the cross-section C-C in Figure 7. The groove bottom is flat but not as much as it was observed for tests performed in surrounding temperature 200°C. Parameter Ra equals 60 nm and Rq equals 68 nm, the distance from maximum peak top to minimum valley bottom is 220 nm. The flat part of wear groove has width of about 75 μm.

Summarizing obtained results, it should be stated that depth of the wear groove increases with increasing surrounding temperature. The flashes around the wear tracks were not observed for surrounding temperature of 350 °C, in contrast to tests performed in other conditions (RT and 200 °C). Their height is comparable to groove depth. For experiments performed at higher temperatures the track bottom becomes flat with small value of Ra = 20.3 nm observed especially for 200°C. For all cases considered, the ball wear can be disregarded as it was very small or simply not observed.

Table V. Groove depths for Tests 7 and 8 temperature 350 ℃

	Test 7	Test 8
Average [μm]	2.23	2.21
Minimum [μm]	1.8	2.1
Maximum [μm]	2.8	2.4
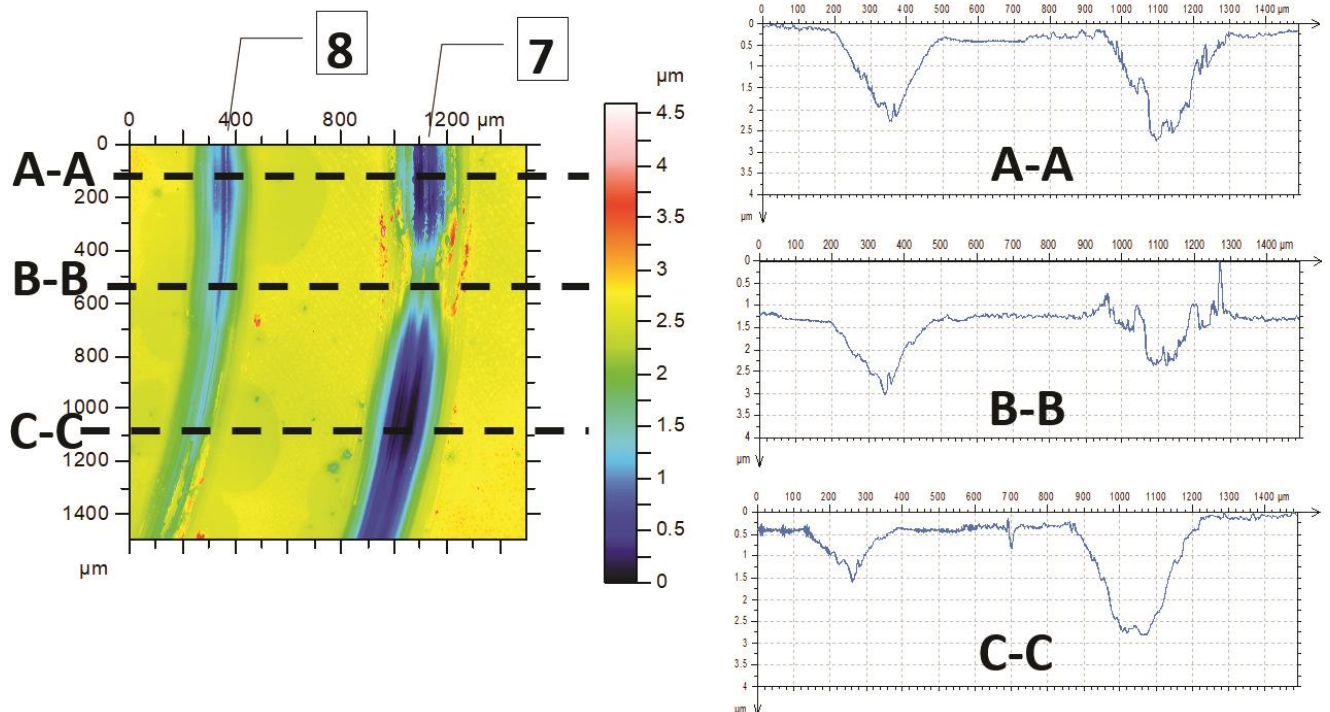
Fig. 7. Roughness topography after ball-on-disk test at temperature 350 °C with indicated grooves from Tests 7 and 8 roughness topography along indicated cross–sections
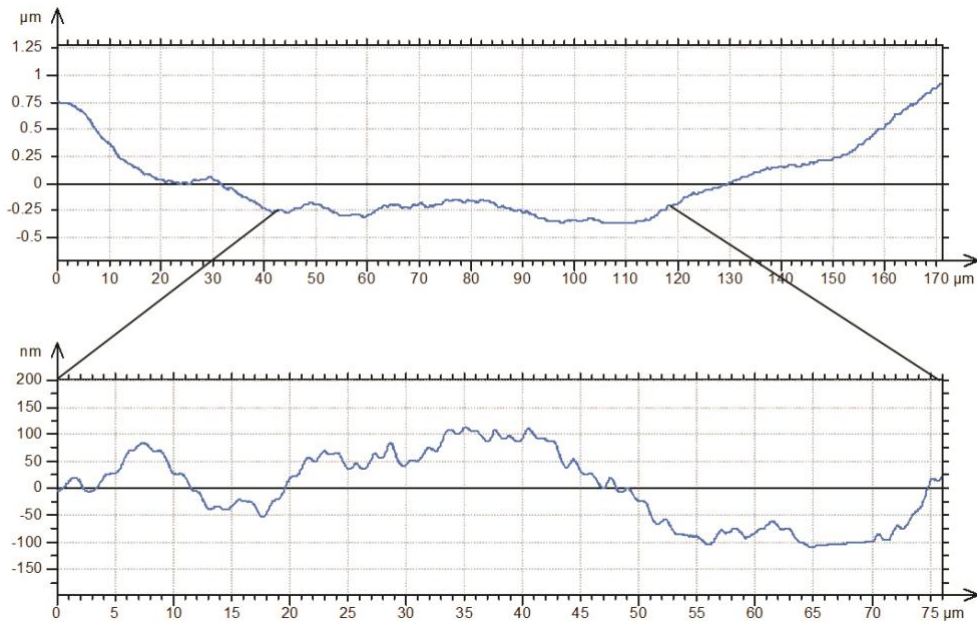
Fig. 8. Cross section C—C through groove bottom for Test 7

Simplified finite element model

Finite element modelling of a typical ball on disc test as presented in Figure 9 is prohibitive from the required computational time. The strongly localised contact stresses combined with induced temperature distribution, wear or oxidation processes can only be captured by high mesh densities in the disc portion under the ball. On the other hand, the actual contact area is only a small fraction of the whole circumferential path made by the ball during the disc rotation. Creating a dense mesh along it would lead to a prohibitive computational cost.
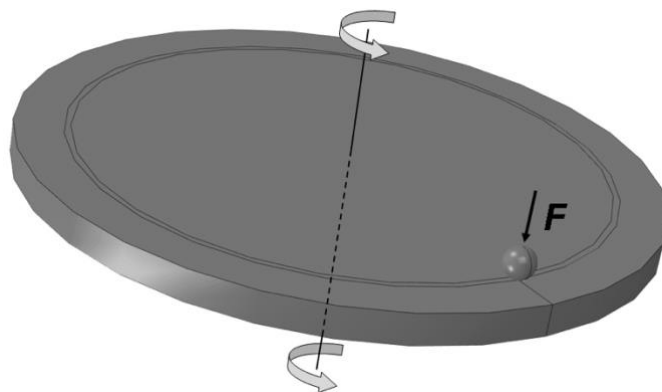
Fig. 9. Ball on disc test

High computational cost can also be related to the long time required for the wear to take place when compared to the time of a single rotation of the disc. An approach allowing to overcome this difficulty is to introduce two computational time scales. In the short time scale, geometrical changes due to wear can be disregarded and one can assume that the system reaches a steady state. This means that the stresses, temperature distribution etc. in the disc follow the ball and in eulerian description do not change with time, when the disc moves under the ball. The steady state in the disc can be found assuming it is made of an elastic material and provided the frictional energy dissipated at contact gives a temperature rise above ambient only in the vicinity of the ball.

Having the solution of the steady state, one can apply it for the second, long time scale and change the contact geometry according to adopted wear kinetics. In the present contribution the steady state condition is the main assumption underlying the finite element mesh creation for the simulation of wear. It allows to consider only a portion of the disc, where the actual stress and temperature changes take place. Figure 10 presents the model of disc and the ball constructed for the simulation. Only half of the ball and disc portion directly underneath is considered. Appropriate boundary conditions are imposed: symmetry conditions

on the plane A-A, heat conduction to the surrounding material through surfaces indicated in red, heat flow into the air through free surfaces. The initial temperature for the disc and the ball is set to 20°C. It is assumed that wear takes place only on the disc side, there is no ball wear. This was indeed the case for the performed ball-on-disc tests.
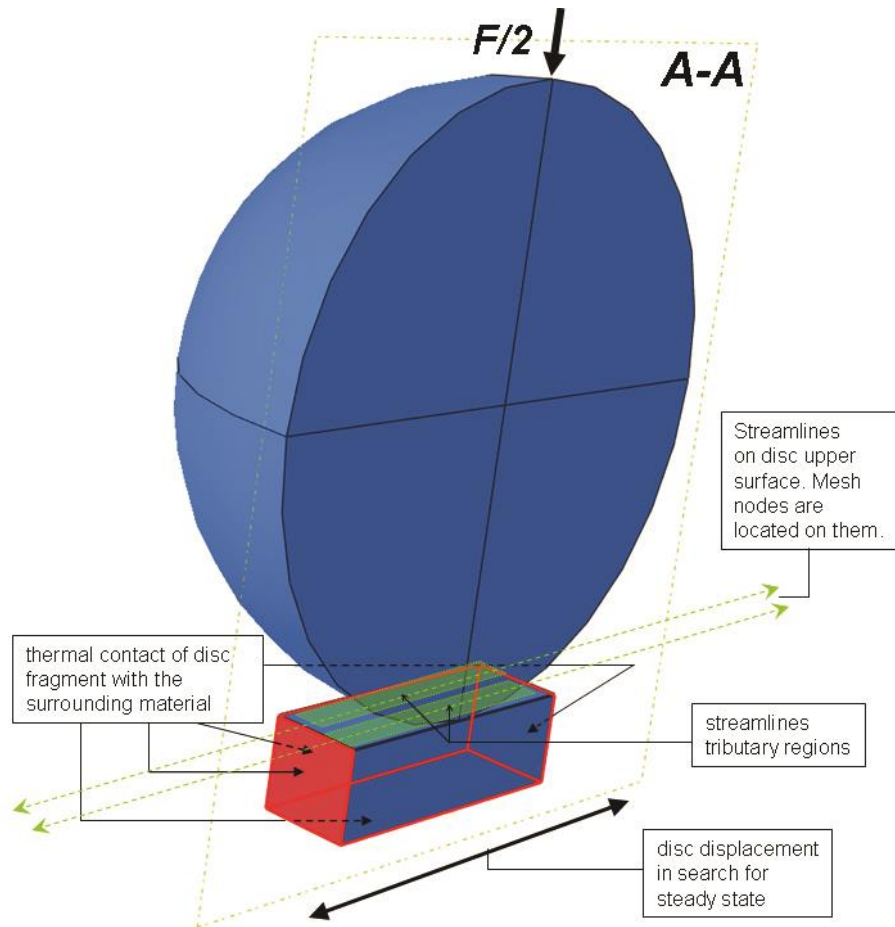
Fig. 10. Simplified model of ball on disc test

To effectively take advantage of the simplified geometry, the following procedure was implemented, allowing for modelling of wear phenomena combined with thermo-mechanical coupling:

STEP 1: press the ball into the disc, perform static analysis;

STEP 2: slide the disc in one direction and reach temperature steady state, perform coupled thermo-mechanical analysis;

STEP 3: taking the steady state temperature and contact stress fields calculate the respective wear rates and change the mesh accordingly, perform static analysis;

STEP 4: to allow for a better search of the new steady state, set the temperature in the disc to the initial temperature of 20°C and keep the ball temperature unchanged, perform coupled thermo-mechanical analysis;

STEP 5: slide the disc in the opposite direction until steady state corresponding to the modified geometry is found, perform coupled thermo-mechanical analysis;

STEP 6: repeat steps (3)-(5) until the desired simulation time is reached.

Although the procedure resembles the reciprocating test, it is closely related to the described ball on disc setup with disc rotating in one direction only. This is achieved through resetting the temperature in the disc to ambient in STEP 4. Elastic response of the disc and the ball guarantees that the subsequent search for steady state can be performed regardless of the actual movement direction of the substrate, the resulting temperature distribution will correspond to the situation of disc undisturbed rotation in one direction only. The situation is similar to that presented in [13].

The rates of wear calculated at the beginning of STEP 3 are kept constant throughout the step. This means that the numerical procedure of integrating the wear kinetics is Euler forward scheme. To obtain the stable solution and accurate results of the entire process, the time duration of STEP 3 should be reasonably small. This implies that the number of repetitions of STEPS 3–5 would normally be high.

The mesh modification and creation of the new contact profile was performed using the adaptive mesh capabilities offered by Abaqus through the user subroutine UMESHMOTION, see [14]. In the following, the calculation algorithm will be presented.

Wear calculation

In the following the wear modeling is applied only for disc surface being in contact with the ball. It is assumed that the there is no ball wear during the simulation. The interaction between the ball and the disc is modelled using friction law

$$\tau = \mu(T)\,\sigma \tag{1}$$

where τ and σ are respectively tangential and normal stresses at contact and μ is the friction coefficient. In our case the friction coefficient is a function of local temperature.

The wear rate is calculated using the Archard relation

$$\dot{W} = \frac{\beta}{H}\tau \upsilon A \tag{2}$$

with W being the volumetric material loss, A the contact area, β the nondimensional wear coefficient, H hardness and υ the sliding velocity.

As indicated in Figure 10, the nodes on the upper surface of the considered disc fragment are placed on straight lines having the same direction as the direction of disc's fragment displacement vector. They create streamlines on which nodal vertical movement will be applied according to the wear rates. Each of the streamlines has the tributary region of the disc upper surface, as presented in Figure 10. These regions comprise the total upper surface of the disc.

By taking advantage of the steady state stress and temperature fields, equation (2) for each streamline can have the form

$$\dot{W} = \int \frac{\beta}{H}\tau(s)\upsilon(s)\omega(s)ds \tag{3}$$

where s indicates a position along the streamline, $\omega(s)$ is the width of the tributary region associated with the streamline.

For the time scale relevant for wear process, the material ablation is assumed to occur uniformly for each streamline and its tributary region and therefore we can write

$$\dot{W} = \int \dot{h}(s)\omega(s)ds = \dot{h}\int \omega(s)ds \tag{4}$$

where h is the thickness of the worn material.

Rewriting expressions (3) and (4) in a discrete form for a given streamline we have

$$\sum_{i=1}^{N}\frac{\beta}{H}\tau_i\upsilon_iA_i = 2\pi r\omega\dot{h} \tag{5}$$

In the above r is the radius of the streamline on disc upper surface and $2\pi r$ is the streamline length. The summation on the right-hand side of the expression is performed over all nodes lying on the given streamline and index i indicates that each quantity is evaluated at node. It has been assumed that the width w of the tributary region remains constant along the streamline. Noting that $A_i = \omega\,\Delta s_i$ from (5) we obtain expression for $\dot{h}$

$$\dot{h} = \frac{\sum_{i=1}^{N}\frac{\beta}{H}\tau_i\upsilon_i\Delta s_i}{2\pi r} \tag{6}$$

where Δs_i is the distance on the streamline associated with node i. The calculated material recession rate $\dot{h}$ is used to modify position of nodes on disc's upper surface along vertical direction during STEP 3 of the described simulation procedure. For STEP 3 of time length Δt the total vertical movement distance for a given streamline is $h = \dot{h}\,\Delta t$. Since $\dot{h}$ is calculated from the steady state fields valid for the beginning of STEP 3, the resulting h complies with Euler forward integration scheme.

Model results

The relevant material parameters of MoS2 film are listed in Table VI and Ti6Al4V substrate in Table VIII. Ball material is aluminum oxide and its properties are listed in Table VII. The relation between the friction coefficient and temperature is assumed in the form

$$\mu(T) = \mu_{max} - (\mu_{max} - \mu_{min})\left(\frac{T - T_{min}}{T_{max} - T_{min}}\right)^{\eta} \tag{7}$$

As presented in Figure 11 it decreases from μ_{max} to μ_{min} as temperature changes from T_{min} up to T_{max}. In equation (7): μ_{max} = 0.2, μ_{min} = 0.05, T_{max} = 200 °C, T_{min} = 0 °C, η = 1. It roughly matches with experimental data presented by Kubart et al. [15]
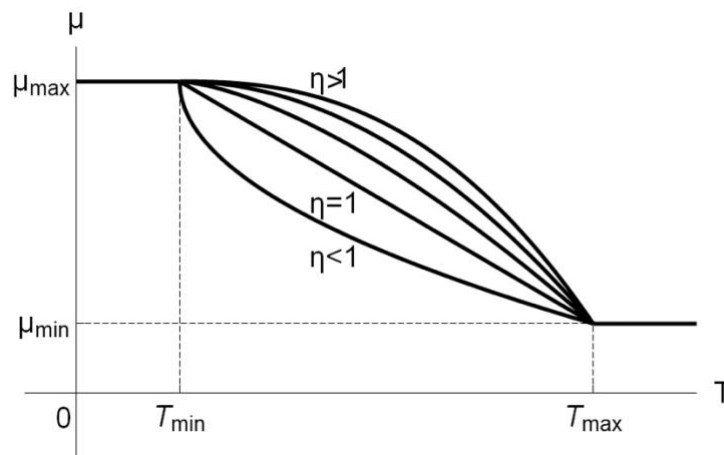
Fig. 11. Relation between friction coefficient and temperature   .

Table VI. Material parameters of MoS2 layer (after [16] and [17])

Young modulus	Poisson's ratio	Density	Specific heat	Thermal conductivity	Thermal expansion coefficient
200 GPa	0.3	5.06 g/cm^3	1.81 J/(cm^{3}K)	0.6 W/(mK)	8.65·10^{-6} 1/C

Table VII. Material parameters of Al2O3 ball

Young modulus	Poisson's ratio	Density	Specific heat	Thermal conductivity	Thermal expansion coefficient
380 GPa	0.3	3.89 g/cm^3	0.88 J/(gK)	30 W/(mK)	8.1·10^{-6} 1/C

Table VIII. Material parameters of Ti2Al4V substrate (after [18])

Young modulus	Poisson's ratio	Density	Specific heat	Thermal conductivity	Thermal expansion coefficient
110 GPa	0.31	4.42 g/cm^3	553 J/(kgK)	7.1 W/(mK)	9.2·10^{-6} 1/C

Figure 12 presents the results of finite element simulation of ball-on-disk experiment compared with wear grooves obtained from ball on disc Tests 1 and 3 described in Section 2. Surrounding temperature in the model equals 20°C and is in line with experimental conditions for this particular group of tests. The ratio β/H present in Equation (6), where β is a nondimensional wear coefficient and H, is material hardness, serves as a proportionality factor for the numerical algorithm coded in Abaqus subroutine UMESHMOTION, see [2]. Its value was assumed to be 2E-13 to fit the numerical results to the experimentally obtained data. We can see satisfactory agreement between the model resulting wear groove and experiment. Numerically obtained shape of the groove is similar to the experimental one, its dimensions are also nicely predicted. There are some aspects that cannot be covered by the present modelling, though. The real track is very uneven with flashes on both sides. Since in the wear model the layer material is assumed to be elastic

only, it is not possible to properly capture the building of flashes. It is also not possible to mimic the roughness of the groove's contour, as it is related to initial (not ideally flat) topography and nonuniform distribution of material properties.

(a)   (b)
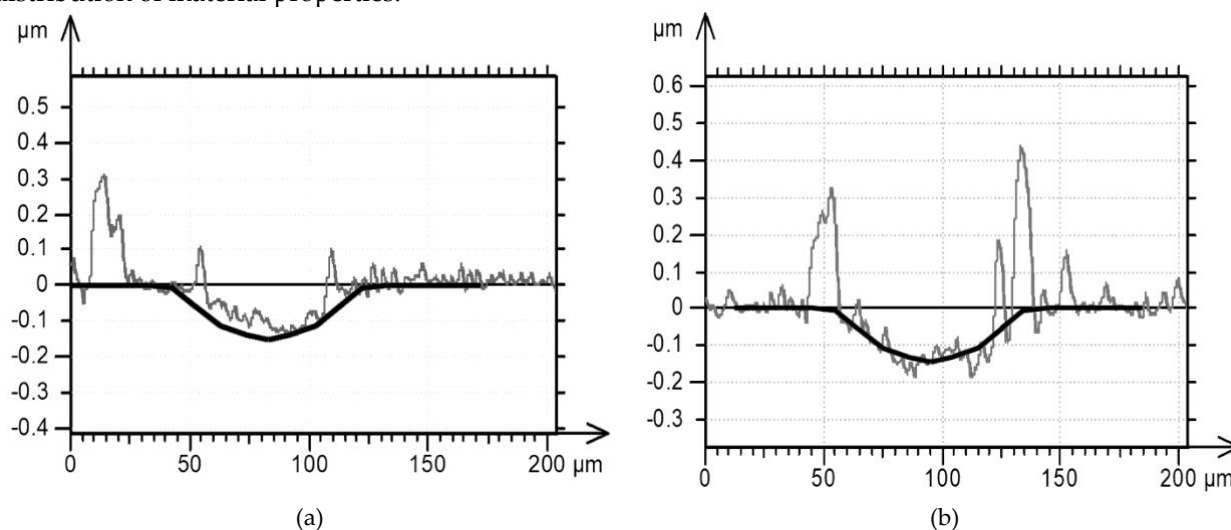
Fig. 12. Model results (thick black line) versus experimental findings. a) Wear groove from ball on disc Test 1. b) Wear groove from ball on disc Test 2

Summary

The paper reports results of unlubricated ball-on-disk wear experiments. The sapphire ball diameter was 6 mm, the substrate was 3 μm thick MoS_2 film deposited on Ti6Al4V material. Three different surrounding temperature conditions were considered, namely 20 °C, 200 °C and 350 °C. Summarizing the tests results it should be stated that depth of the wear groove increases with increasing surrounding temperature. As expected, it is also proportionally affected by ball loading. The flashes around the wear tracks are not observed for surrounding temperature of 350°C, in contrast to tests performed in other conditions (RT and 200 °C), where height of flashes is comparable to groove depth. For experiments performed at 200 °C and 350 °C the track bottom becomes flat with small value of Ra = 20.3 nm observed especially for 200 °C. After 20000 cycles the flat part of wear groove has width of about 70 nm.

In the finite element modeling part of the paper wear phenomena during ball on disc test is numerically analyzed. The created FE model includes thermo-mechanical simulation of frictional sliding and wear process simulated by Archard equation. The numerically obtained shape of the wear groove resulting from wear modeling is compared with wear tracks obtained during room temperature ball-on-disk experiments. They match quit well with the experimental data, although some experimental aspects cannot be captured. It is not possible to mimic the building of flashes and the roughness of the groove's contour. This roughness is related to initial topography and nonuniform distribution of coating material properties.

References

[1] Kucharski S., Mróz Z., Identification of wear process parameters in reciprocating ball-on-dic test, *Tribology International*, 2011, Vol. 44(2), 154-164.

[2] Sadowski P., Stupkiewicz S., A model of thermal contact conductance at high real contact area fractions, *Wear*, 2010, Vol. 268, 77-85.

[3] Sadowski P., Stupkiewicz S., Friction in lubricated soft-on-hard, hard-on- soft and soft-on-soft sliding contacts, *Tribology International*, 2019, Vol. 129, 246-256.

[4] Paczelt I., Mróz Z., Analysis of thermo-elastic wear problems, *Journal of Thermal Stresses*, 2011, Vol. 34, 569–606.

[5] Paczelt I., Mróz Z., Numerical analysis of steady thermo-elastic wear regimes induced by translating and rotating punches, *Computers and Structures*, 2011, Vol. 89, 2495–2521.

[6] Paczelt I., Kucharski S., Mróz Z., The experimental and numerical analysis of quasi-steady wear processes for a sliding spherical indenter, *Wear*, 2012, Vol. 274– 275, 127–148.

[7] Kucharki S., Starzyński G. Study of contact of rough surfaces: Modeling and experiments, *Wear*, 2014, Vol. 311, 167-179.

[8] Mróz Z., Kucharski S., Paczelt I. Anisotropic friction and wear rules with account for contact state evolution. *Wear*, 2018, Vol. 396-397, 1–11.

[9] Hirvonen J.-P., Koskinen J., Jervis J., Nastasi M. Present progress in the development of low friction coatings, *Surface and Coatings Technology*, 1996, Vol. 80, 139–150.

[10] Arlsan E., Buelbuel F., Alsaran A., Celik A., Efeoglu, I. The effect of deposition parameters and Ti content on structural and wear properties of MoS2Ti coatings, *Wear*, 2005, Vol. 259, 814–819.

[11] Moskalewicz T., Zimowski S., Wendler B., Nolbrzak P., Czyrska-Filemonowicz A. Microstructure and tribological properties of low-friction composite MoS2(Ti,W) coating on the oxygen hardened Ti-6Al-4V alloy, *Metals and Materials International*, 2014, Vol. 20, 269–276.

[12] Furlan K., de Mello J., Klein A. Self-lubricating composites containing MoS2: A review, *Tribology International*, 2018, Vol. 120, 280–298.

[13] Lengiewicz J., Stupkiewicz S. Efficient model of evolution of wear in quasi- steady-state sliding contacts, *Wear*, 2013, Vol. 303, 611–621.

[14] Deassault Systemes. ABAQUS version 6.7, User documentation, 2007.

[15] Kubart T., Polcar T., Kopecky L., Novak R., Novakova D. Temperature dependence of tribological properties of MoS2 and MoSe2 coatings, *Surface and Coatings Technology*, 2005, Vol. 193, 230–233.

[16] Mclaren. Thermal conductivity anisotropy in molybden disulfide films. PhD thesis, University of Illinois at Urbana-Champaign, Urbana

[17] Donnet C., Martin J., Le Mogne T., Belin M. Super-low friction of MoS2 coatings in various environments, *Tribology International*, 1996, Vol. 29, 123-128.

[18] Murr L., Esquivel E., Quinones S., Gaytan S., Lopez M., Martinez E., Medina F., Hernandez D., Martinez E., Martinez J., Stafford S., Brown D., Hoppe T., Meyers W., Lindhe U., Wicker R. Microstructures and mechanical properties of electron beam-rapid manufactured Ti-6Al-4V biomedical prototypes compared to wrought Ti-6Al-4V, *Materials Characterization*, 2009, Vol. 60, 96-105.